TRANSACTIONS OF THE INSTITUTE OF AVIATION
No. 1(242), pp. 36-56, Warsaw 2016
DOI: 10.5604/05096669.1202201

ISSN 0509-6669
eISSN 2300-5408

SIMULATION INVESTIGATION OF AERODYNAMIC EFFECTIVENESS REDUCTION OF HELICOPTER TAIL ROTOR

JAROSŁAW STANISŁAWSKI
Institute of Aviation, al. Krakowska 110/114, 02-256 Warsaw, Poland, jaroslaw.stanislawski@ilot.edu.pl

Abstract

Paper presents the results of the simulation tests concerning the performance of the tail rotor in the directional maneuver of the helicopter due to the flow changes of the tail rotor blades. The calculation model includes the yawing of the helicopter fuselage and motion of the tail rotor blades treated as the set of the deformable elastic axes with distributed lumped mass. The equations of motion of the tail rotor blades are solved by applying Runge-Kutta method taking into account the bending and torsion eigen modes of the blades. The results of the calculations indicate occurrence of the significant changes of the tail rotor thrust during directional maneuver of the helicopter in case of side wind or influence of the main rotor vortices.
Keywords: helicopter, tail rotor, aerodynamic effectiveness.

1. INTRODUCTION

The majority of helicopters is built in configuration which consists of the main rotor and the tail rotor for the directional control and stability. During helicopter operations some accidents have happened which were thought to be connected with loss of direction control. Investigations did not confirm that reasons of the repeating accidents might be mechanical damage of control system or other important part of helicopter structure. Additionally the accidents have occurred at the good weather conditions. The more exact analysis of the circumstances of the accidents turns attention to the disturbances of the airflow of the tail rotor blades, which influences the amount of generated thrust. In some flight conditions the phenomenon of loss of tail rotor aerodynamic effectiveness (LTE) for helicopter can occur. In Fig. 1 were shown the conditions, which due to direction of airflow the possibility of loss of the tail rotor effectiveness rises.

The disadvantageous direction of the airflow from the left affects the helicopter with counter-clock rotation of the main rotor and with advancing blade located at the right side of the fuselage. In the case of helicopters with the main rotors of clock rotation the loss of tail rotor aerodynamic effectiveness happens for airflow from the right side.

The rate of helicopter accidents associated with loss of the directional control was so high that in the nineties of 20th century the American FAA issued Advisory Circular 90-95 [1] including the exact description of the phenomenon of loss of the tail rotor aerodynamic effectiveness and also including recommendations and instructions for pilots which allow to limit the potentially

dangerous situations. Information about conditions-increasing the possibility of loss of the tail rotor effectiveness were collected in EASA documents concerning safety of flight [2], [3] and edited by FAA in rotor craft flying handbook [4]. Instructions concerning avoidance of circumstances of high risk of loss of the tail rotor effectiveness were defined in requirements for helicopter operators published by UK Civil Aviation Authority [5]. An article for larger group of readers, focused on LTE phenomenon was published in Flight International [6], which discussed the main reasons of LTE threats. Detailed information on circumstances of helicopter accident which were thought to be connected with LTE were published in papers of aviation organizations [7], [8] and US administration [9].

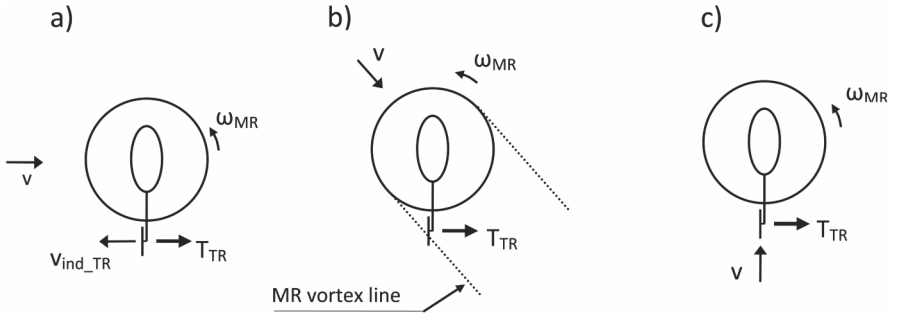

Fig. 1. Helicopter flight conditions increasing possibility of reduction the aerodynamic effectiveness of tail rotor (TR – tail rotor, MR – main rotor): a) side flight, wind gusts, b) flight in range of directions where interference of the main rotor wake may occur, c)back ward flight [Author, 2015]

Applying simulation method for investigation of loss of the tail rotor effectiveness allowed for a better definition of conditions when that phenomenon may occur. The French team of ONERA [10] used modified program code HOST (Helicopter Overall Simulation Tool) enabling research of the tail rotor airflow, conditions of high influence of the main rotor wake on tail planes and generation of vortex ring state on tail rotor. This paper presents results of simulation calculations concerning work of tail rotor of light helicopter in the following cases: side wind gusts in hover conditions, in the level flight at low speed the main rotor vortex passage through the tail rotor area. In both cases the motion of helicopter is assumed without the control corrections introduced by pilot. The calculations were also conducted for directional maneuver of helicopter in the level flight at low speed conditions with introduced control function of the tail rotor blade pitch. The simulations of tail rotor action were performed by applying modified version of program codes developed at the Institute of Aviation used for calculations of the rotor blade loads.

2. MODEL OF TAIL ROTOR IN MANEUVER

The calculation model applied for simulation of the tail rotor action in the helicopter directional maneuvers consists of the following components:

- the stiff fuselage able to yaw around the axis of the main rotor shaft,
- the tail rotor treated as set of elastic blades with possibility of applying the function pitch angle control,
- for conditions of forward flight the simplified model of the main rotor wake applied in form of two vortex lines generated behind the main rotor (Fig 1b).

The additional assumption are applied to define the fuselage and tail rotor motion:

- during directional maneuver the helicopter centre of mass stays in place or moves uniformly without accelerations,

- angular speeds of the main and tail rotors are constant at the directional maneuver,
- changes of the tail rotor thrust affect only parameters of the fuselage rotary motion around axis of the main rotor shaft,
- the changing parameters of helicopter yaw motion affect the airflow conditions of the tail rotor blades.

Considering the equation of rotation motion of fuselage the following components were included: torque of the main rotor, yawing aerodynamic moment of the fuselage, yawing moment of the tail rotor hub, variable thrust of the tail rotor as result of the following factors: blade pitch control, changes of blade airflow due to fuselage motion and interference of main rotor vortices. The simplified equation of motion of fuselage during directional maneuver of helicopter is as follows:

$$I\ddot{\beta}_f = M_{mr} + M_f + T_{tr} \cdot L_{tr} + M_{ytr} \tag{1}$$

where
I – fuselage mass moment of inertia relative to axis of the main rotor shaft,
M_{mr} – torque of the main rotor,
$M_f(\beta_f)$ – yawing aerodynamic moment of the fuselage,
$T_{tr}(\beta_f,\varphi)$ – tail rotor thrust,
L_{tr} – distance between axes of the main rotor and the tail rotor,
$M_{ytr}(\beta_f,\varphi)$ – yawing moment of the tail rotor hub,
β_f – yaw angle of the fuselage,
φ – pitch angle of the tail rotor blades.

The equation of motion of the helicopter fuselage (1) is solved for time interval equal to a few seconds. At this time the tail rotor performs a few hundreds of revolutions. The time step increment for solution of the equation of fuselage motion is assumed equal to the period of one revolution of the tail rotor. For the time step of solution the equation of motion (1) the constant values of forces and moments are applied, which in the case of the tail rotor thrust T_{tr} and tail rotor hub yawing moment M_{ytr} are assumed equal to the average values for the period of one revolution of the tail rotor. Instantaneously during one revolution values of thrust, yaw moment and other parameters of the tail rotor are computed with time step coincident with change of the azimuth position of blade on the tail rotor disk equals angle $\Delta\psi = 5^o$ which gives the set of 72 results for each blade per one revolution of rotor.

In the simulation cycle the calculation results of the fuselage yaw motion and loads of the tail rotor blades are exchanged between two computing procedures. The temporary values of the fuselage yaw motion parameters: the angular acceleration, the angular velocity and the yaw angle are sent to the procedure computing the tail rotor thrust with the actualization rate equal the time of one tail rotor revolution. For changing airflow conditions at all considered azimuth positions of blades the loads of each blade and the whole tail rotor are calculated. The parameters of the fuselage motion during one tail rotor revolution are assumed constant. After completing the tail rotor revolution the new mean values of the tail rotor thrust and yaw moment are sent to the procedure computing the fuselage motion. At the next step the results of calculation of the fuselage yaw motion are applied as the input data for computing the tail rotor loads in changed conditions.

The model of the tail rotor blade shown in Fig. 2 is treated as a structure which consists of elastic axis with distribution of lumped masses. Solution of the equations of motion of elastic blades takes into account mutual twist, bent in-plane and bent out-of-plane deflections of blade

elastic axes. The equations of blade motion are solved using Runge-Kutta method and applying Galerkin method which assumes that deflections of blade are equal to the sum of variable with time components deriving from considered eigen modes of tail rotor blade.

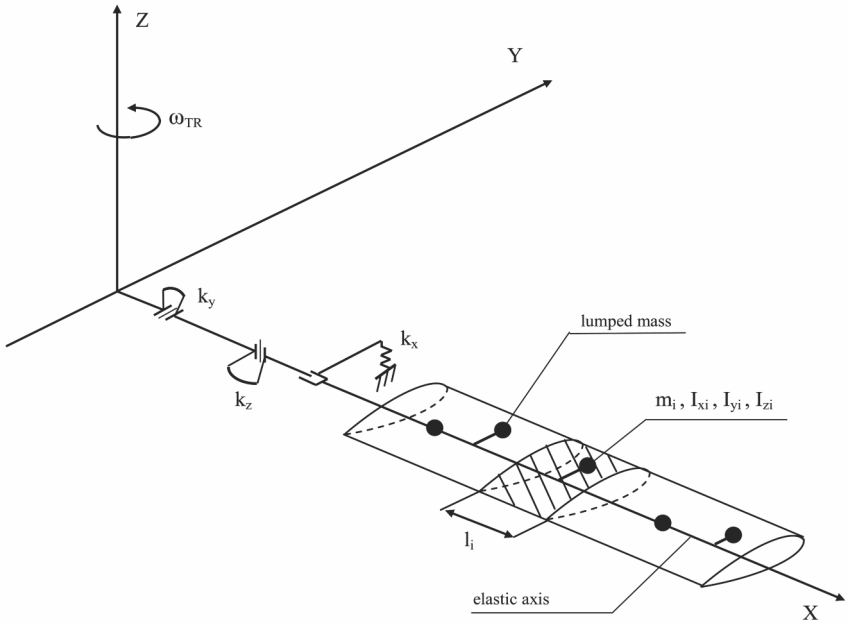

Fig. 2. Physical model of tail rotor blade with section of l_i length, mass m_i and moments of inertia I_{xi}, I_{yi}, I_{zi} replaced by lumped mass [Author, 2015]

The equations of motion of rotating elastic axis for y bending in-plane deflections, z bending out-of-plane deflections and φ torsion deflections are as follows:

$$\int_0^R m(x)\ddot{y}\,dx + \int_0^R \left\{ \frac{d^2}{dx^2}\left[EJ_Z \left(\frac{d^2 y}{dx^2} \right) \right] - \frac{d}{dx}\left(N \frac{dy}{dx} \right) + m(x)\omega_{TR}^2 y \right\} dx = \int_0^R \left(F_{Y_{EX}} - F_{Y_{IN}} \right) dx \tag{2a}$$

$$\int_0^R m(x)\ddot{z}\,dx + \int_0^R \left\{ \frac{d^2}{dx^2}\left[EJ_Y \left(\frac{d^2 z}{dx^2} \right) \right] - \frac{d}{dx}\left(N \frac{dz}{dx} \right) \right\} dx = \int_0^R \left(F_{Z_{EX}} - F_{Z_{IN}} \right) dx \tag{2b}$$

$$\int_0^R I_X(x)\ddot{\varphi}\,dx + \int_0^R \frac{d}{dx}\left[GJ_X \left(\frac{d\varphi}{dx} \right) \right] dx = \int_0^R \left(M_{S_{EX}} - M_{S_{IN}} \right) dx \tag{2c}$$

where

$F_{Y_{EX}}, F_{Z_{EX}}, M_{S_{EX}}$ – shear forces and torsion moment of external loads acting on segment dx of elastic axis,

$F_{Y_{IN}}, F_{Z_{IN}}, M_{S_{IN}}$ – inertial forces and torsion moment of inertial forces reduced respectively by following components $m\ddot{y}, m\ddot{z}, I_X\ddot{\varphi}$ acting on segment dx of elastic axis,

the centrifugal forces per length acting on segment *dx* of rotating elastic axis are as follows

$\frac{d}{dx}\left(N\frac{dz}{dx}\right)$ – out-of-plane

$\frac{d}{dx}\left(N\frac{dy}{dx}\right)-m(x)\omega_{TR}^2 y$ – in-plane

where

$N=\int_r^R m(x)\omega_{TR}^2 x dx$ – local centrifugal force at cross-section located at distance *r* from axis of the rotor shaft.

According to Galerkin method it is assumed that deflections of the elastic axis *y, z, φ* are equal to superposition of modal components:

$$y(x,t)=\sum_{i1=1}^{I1}\rho_{i1}(t)y_{i1}(x);\ z(x,t)=\sum_{i2=1}^{I2}\delta_{i2}(t)z_{i2}(x);\ \varphi(x,t)=\sum_{i3=1}^{I3}\eta_{i3}(t)\varphi_{i3}(x) \tag{3}$$

where

y_{i1}, z_{i2}, φ_{i3} – eigen modes respectively bending in-plane, bending out-of-plane, and torsion;
ρ_{i1}, δ_{i2}, η_{i3} – time dependent shares of each eigen mode, which are determined in computing process;
$I1$, $I2$, $I3$ – numbers of considered bending and torsion eigen modes.

Applying orthogonality condition for the eigen modes each of equations (2) can be converted into sets of equations (4a, 4b, 4c), where each equation can be treated as equation of oscillating motion of an equivalent structure of a single degree of freedom. The frequencies of considered eigen modes of blade are equal respectively frequencies of eigen modes of equivalent structures of one degree of freedom:

$$\ddot{\rho}_{i1}+\rho_{i1}p_{i1}^2=Q_{Y_{i1}},\ i1=1,...,I1 \tag{4a}$$

$$\ddot{\delta}_{i2}+\delta_{i2}f_{i2}^2=Q_{Z_{i2}},\ i2=1,...,I2 \tag{4b}$$

$$\ddot{\eta}_{i3}+\eta_{i3}\nu_{i3}^2=Q_{\varphi_{i3}},\ i3=1,...,I3 \tag{4c}$$

where

p_{i1}^2, f_{i2}^2, ν_{i3}^2 – square of blade eigen mode frequencies for bending in-plane, out-of-plane and torsion,

$Q_{Y_{i1}}$, $Q_{Z_{i2}}$, $Q_{\varphi_{i3}}$ – generalized forces for considered eigen modes of the tail rotor blade.

The equations of motion (4) of equivalent masses of one degree of freedom can be solved using Runge-Kutta method. For given moment of time the parameters of blade motion are determined as sum of contributions (3) of considered blade eigen modes.

Aerodynamic forces acting on segment of blade at given azimuth position on the tail rotor disk are computed applying the blade element theory. The local angle of attack at blade cross-section depends on temporary conditions of airflow:

$$\alpha=\vartheta_{contr}+\varphi_g+\Delta\varphi-arc\ tg\left(\frac{u_Z}{u_X}\right), \tag{5}$$

where
ϑ_{ster} – pitch angle due to control,
φ_g – geometric twist,
$\Delta\varphi$ – torsion deformation,
u_z, u_x – out-of-plane and in-plane components of the cross-section airflow of the tail rotor blade including the effects of the fuselage yaw motion and the main rotor wake.

The velocity induced by the main rotor wake may strongly affects the components of airflow of the tail rotor blades. For forward flight conditions the wake of the main rotor can be represented by the line elements which in simplified form creates two vortex lines located behind the main rotor (Fig. 1b). It is assumed that circulation associated to simplified vortex line mainly depends on strong tip vortex of blade of the main rotor.

The distribution of velocity induced by vortex lines is defined in accordance to Biot-Savart law. Scheme of segment geometry of vortex line and induced velocity is shown in Fig. 3, where beginning of segment is located at point *B* and its end is located at point *E*. At length of segment is applied the constant circulation Γ_i. In vicinity of vortex segment at point J is induced velocity V_{ij} perpendicular to the plane defined by points *B*, *E* and *J*. The induced velocity can be calculated according to relation (6):

$$V_{ij} = \frac{\Gamma_i}{4\pi h_{ij}} \left(\cos\alpha_2 - \cos\alpha_1\right) \tag{6}$$

The circulation Γ_i of vortex line is assumed as function of airflow parameters at blade tip of the main rotor:

$$\Gamma_i = 0{,}5 \cdot k \cdot b \cdot \frac{\partial c_z}{\partial \alpha} \cdot \alpha \cdot \Omega \cdot R\,, \tag{7}$$

where
k – number of the rotor blades,
b – chord of the blade,
Ω – rotational speed of the main rotor,
R – radius of the main rotor,
α – attack angle at the tip of the blade.

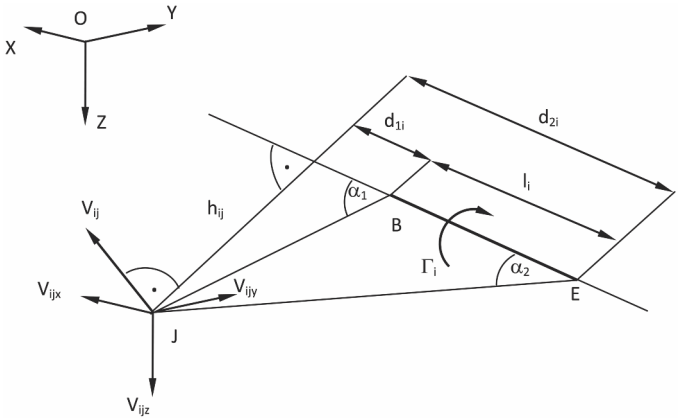

Fig. 3. Scheme of geometry defining velocity induced by segment of vortex line with assigned Γ_i circulation [Author, 2015]

The simulated computations enable to obtain information concerning the changes of load level and range of blade deflections due to azimuth position of blade on the tail rotor disk. The characteristic azimuth of blade positions are shown in Fig. 4, where:

- azimuth 0° is for back horizontal position,
- azimuth 90° for advancing blade at bottom position,
- azimuth 180° at forward horizontal blade position,
- azimuth 270° for retreating blade at top position.

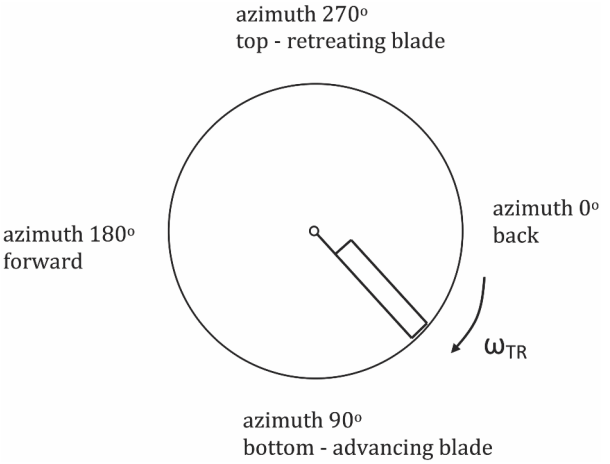

Fig. 4. Location of the characteristic blade azimuth on the tail rotor disk [Author, 2015]

3. SIMULATION RESULTS OF HELICOPTER MANEUVERS

The simulation investigations of the tail rotor operation in conditions of threat of loss of the tail rotor effectiveness were performed for data of light helicopter of 1100 kg mass with three-bladed main rotor and five-bladed tail rotor. The calculations of the helicopter directional maneuver were executed for the following cases:

- in hover conditions the side wind gusts at speed of $V_{gust} = \pm 9$ m/s with constant pitch of the tail rotor blades (no action of pilot), direction of gust wind opposite to induced velocity of the tail rotor (Fig. 5÷8), direction of gust coincident with the tail rotor induced velocity (Fig. 9÷11);
- in level flight at speed of $V = 10$ m/s the slow passage of the main rotor vortex line in vicinity of the tail rotor area, no action of pilot (Fig. 12÷16);
- in level flight at speed of $V = 10$ m/s the directional maneuvers with controlled at quick rate the pitch of the tail rotor blade with initial decreasing of blade pitch (Fig. 17÷19), and with initial increasing of blade pitch (Fig. 20÷25).

In Fig. 5 the thrust and power of the tail rotor are presented for hover conditions with the side wind gust at speed of $V_{gust} = -9$ m/s in direction opposite to the induced velocity of the tail rotor. For the initial value of the tail rotor thrust providing the state of equilibrium in hover the side gust was introduced at 25th revolution of the tail rotor shaft. The whole solution covers 300 revolutions of the tail rotor shaft, which corresponds to time of 4.5 seconds. In Fig. 5a,b after vanishing the initial conditions the rapid increment of thrust and power of tail rotor can be noticed after the gust occurrence. The gust of opposite direction to induced velocity of the tail rotor increases the angles of attack for cross-sections of the tail rotor blades which results in temporary increment of its

thrust about 500 N and power over 2 kW. For the main rotor with counter-clock rotation increment of the tail rotor thrust over balance value causes rotation of the fuselage to the left (Fig. 6a,b). The changes of airflow of the tail rotor blades as the result of fuselage rotation give decrease of thrust and power of the tail rotor. The torsion deflection and angle of attack at tip of tail rotor blade are shown in Fig. 7a,b. For the blade pitch kept constant the all changes of angle of attack are connected with variable airflow conditions of the tail rotor blades due to gust. The noticeable decrease of oscillations in the time runs of torsion deflection and angle of attack about 230th revolution of the tail rotor shaft (for time $t = 3.5$ s) can be thought as result of temporary decrease of the fuselage rotation speed to null value $\omega_{fus} = 0$ (Fig. 6a). In Fig. 8 is shown the map of attack angle distribution on the tail rotor disk for the 100th revolution of the tail rotor shaft. The slightly modified circular shape of the izolines of constant value of attack angles can be noticed.

In Fig. 9, 10 and 11 are presented the time runs of the tail rotor parameters for helicopter rotation in hover with the right side wind gust at speed $V_{gust} = 9$ m/s in coincident direction with the induced velocity of the tail rotor. In this case after gust at the 25th rotor revolution as the result of the decrease of the blade angles of attack (Fig. 11b) also the thrust and power of the tail rotor were diminished (Fig. 9a,b). The thrust of the tail rotor smaller than value of balance caused the increasing turn of the fuselage to the right. Next, without any action of the pilot, the thrust and power of the tail rotor increased over the value of balance due to changing the blade airflow conditions during turn of helicopter. In the right turn the helicopter reached the yaw angle of 120° and then the helicopter began the opposite turn to the left.

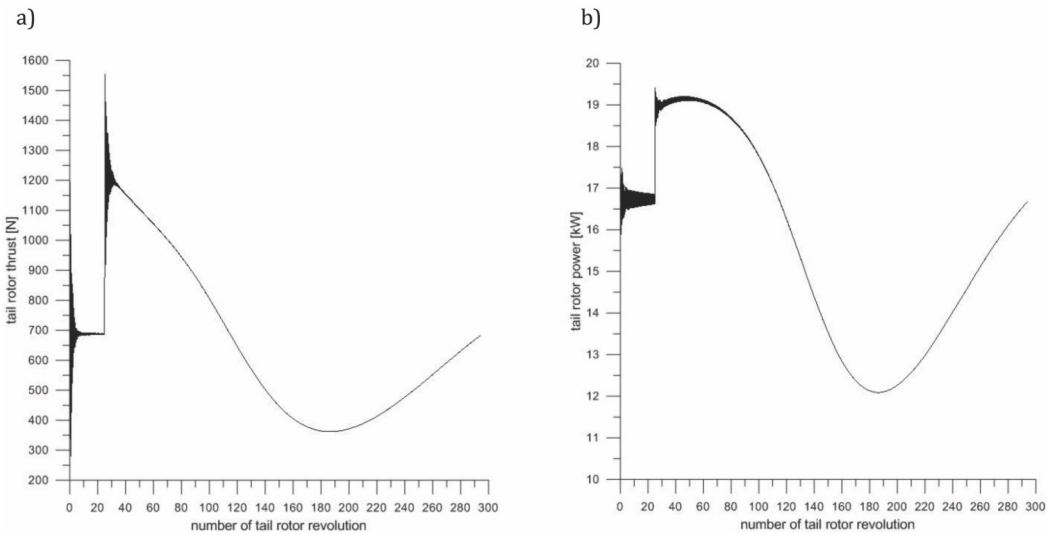

Fig. 5. Changes of thrust (a) and power (b) of the tail rotor in hover with side wind gust at speed of V_{gust} = -9 m/s in direction opposite to induced velocity of tail rotor, no action of pilot, (+) for the tail rotor thrust toward azimuth 90° of the main rotor. The gust beginning at 25th revolution of the tail rotor shaft [Author, 2015]

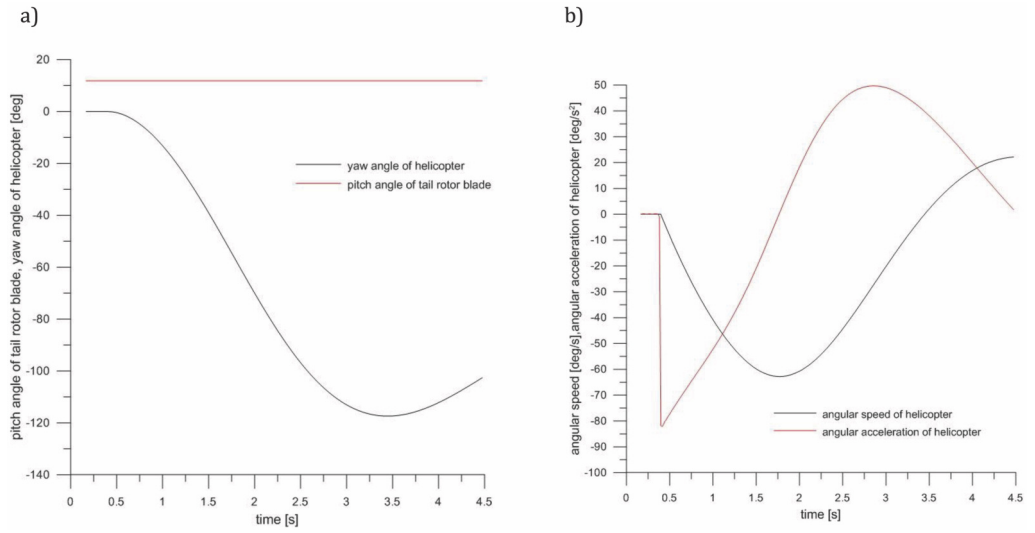

Fig. 6. Changes of yaw angle (a), yaw angular speed and acceleration of helicopter (b) in hover with side wind gust at speed of V_{gust} = -9 m/s in direction opposite to induced velocity of the tail rotor. No action of pilot (constant pitch of the tail rotor blades), yaw angle (-) for rotation of fuselage nose to the left. The gust beginning at 25th revolution of the tail rotor shaft (time t = 0.375 s) [Author, 2015]

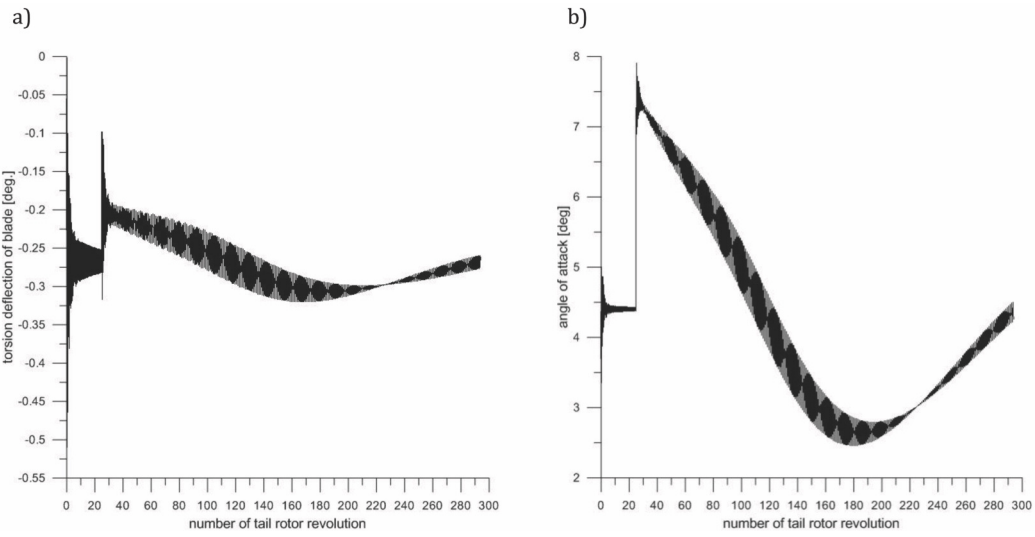

Fig. 7. Torsion deflection (a) and angle of attack (b) at tip of tail rotor blade. Conditions for hover with side wind gust at speed of V_{gust} = -9 m/s in direction opposite to induced velocity of tail rotor. No action of pilot (constant pitch of the tail rotor blades). Torsion deflection (+) for upward rotation of nose of blade cross-section. The gust beginning at 25th revolution of the tail rotor shaft [Author, 2015]

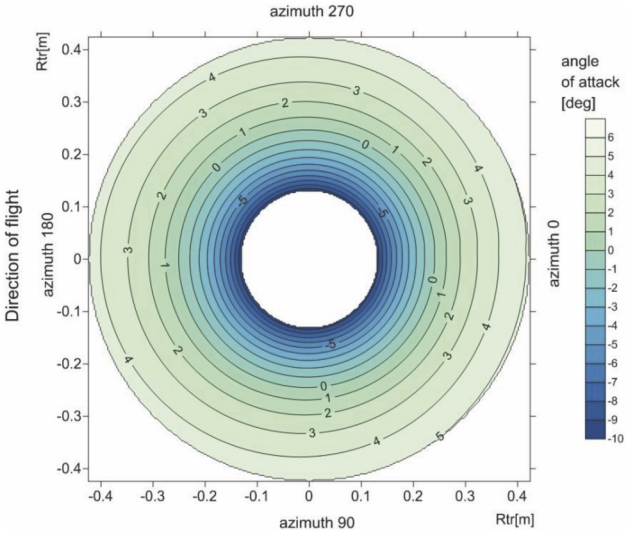

Fig. 8. Distribution of local angle of attack at the tail rotor disk in hover conditions with side wind gust V_{gust} = -9 m/s in opposite direction to induced velocity of tail rotor, no action of pilot. Map for the 100th revolution of the tail rotor shaft [Author, 2015]

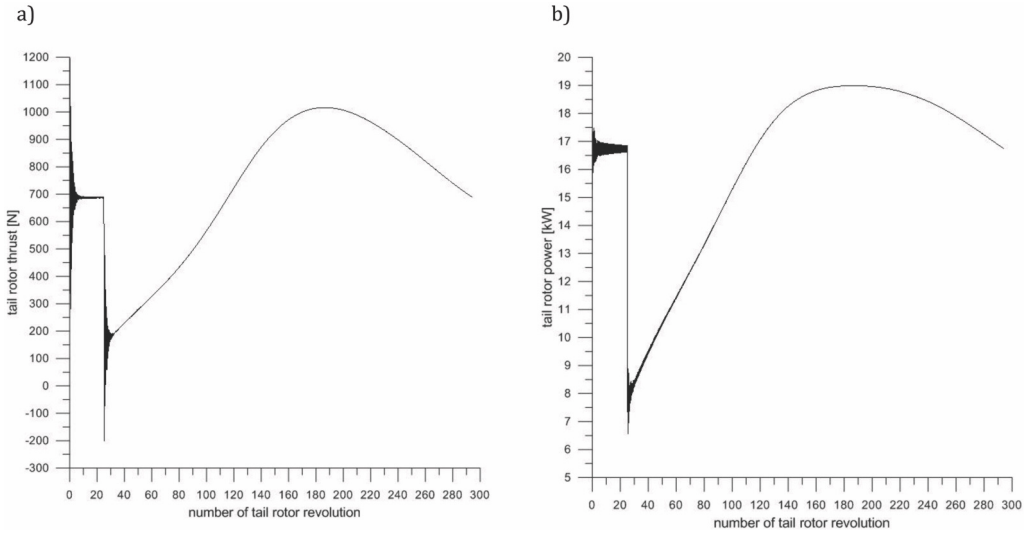

Fig. 9. Changes of thrust (a) and power (b) of the tail rotor in hover with side wind gust at speed of V_{gust} = 9 m/s in direction coincident with induced velocity of the tail rotor, no action of pilot, (+) for the tail rotor thrust towards azimuth 90° of the main rotor. The gust beginning at 25th revolution of the tail rotor shaft [Author, 2015]

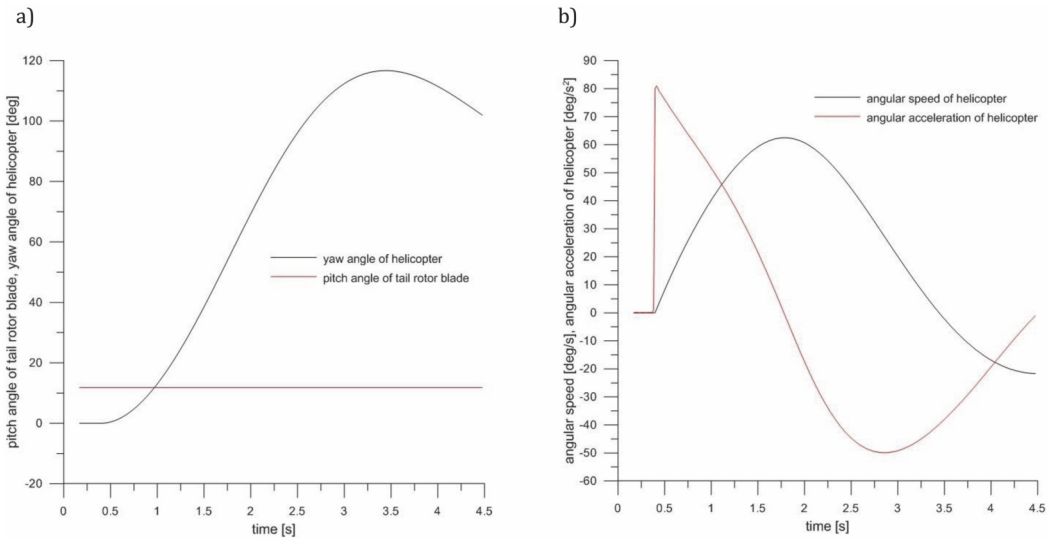

Fig. 10. Changes of yaw angle (a), yaw angular speed and acceleration of helicopter (b) in hover with side wind gust at speed of V_{gust} = 9 m/s in direction coincident with induced velocity of the tail rotor. No action of pilot (constant pitch of the tail rotor blades), yaw angle (+) for fuselage nose turn to the right. The gust beginning at 25th revolution of the tail rotor shaft (time t = 0.375 s) [Author, 2015]

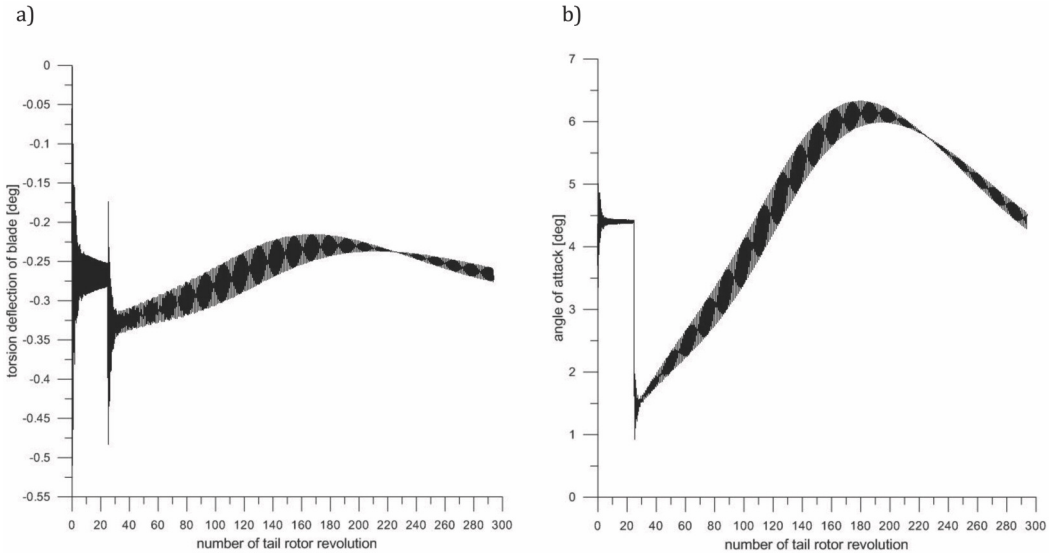

Fig. 11. Torsion deflection (a) and angle of attack (b) at tip of tail rotor blade. Conditions for hover with side wind gust at speed of V_{gust} = 9 m/s in direction coincident with induced velocity of tail rotor. No action of pilot(constant pitch of the tail rotor blades). Torsion deflection (-) for downward turn of nose of blade cross-section. The gust beginning at 25th revolution of the tail rotor shaft [Author, 2015]

The next simulated case in the level flight at speed of $V = 10$ m/s concerns the slow passage of the vortex line generated by the main rotor in the vicinity of the tail rotor area. The vortex line was assumed to gradually approach the vicinity of the tail rotor disk passing over the blade at position of azimuth 270° (Fig. 12). The change of the location of the main rotor vortex line was assumed at angle of 0.01° for one step of blade azimuth change $\Delta\psi = 5°$, what corresponds the increment of location angle of the vortex line $\Delta\beta_{vor\_line} = 0.72°$ for one revolution of the tail rotor shaft. The simulation started with the main rotor vortex line in the parallel position to the longitudinal axis of the fuselage. After 100÷130 revolutions of the tail rotor (time of simulation 1.5÷1.95 s) the vortex line passed through the tail rotor plane over blade tips.

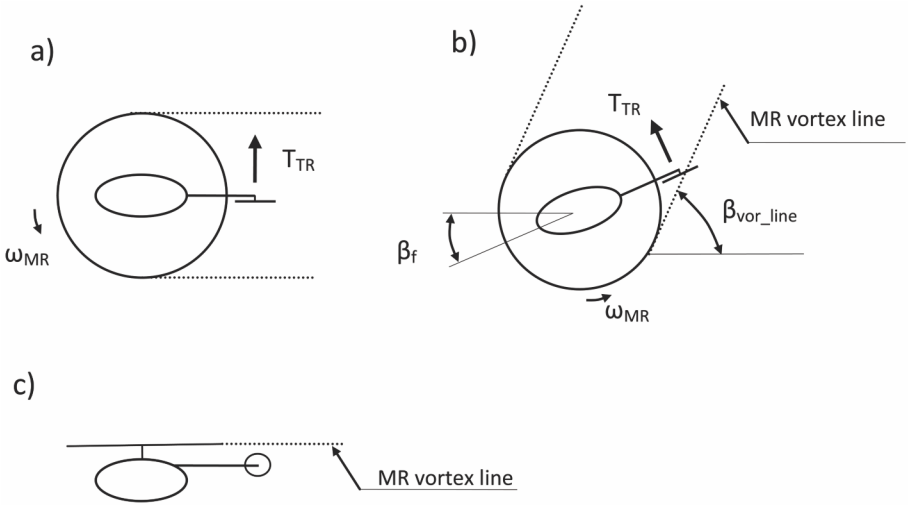

Fig.12. Scheme of position of the main rotor vortex line relative to tail rotor: a) upper view – initial position of fuselage and vortex lines, b) upper view – vortex line is passing through plane of tail rotor of turning helicopter, c)side view – vortex line above tail rotor disk. [Author, 2015]

In Fig. 13 are shown the changes of the tail rotor thrust caused by passage of the main rotor vortex line in the vicinity of the tail rotor. During simulation at the range of 100th÷130th shaft revolution appeared reduction of the tail rotor thrust despite keeping the blade pitch constant and lack of the gusts. The decrease of thrust and associated reduction of the tail rotor power (Fig. 14) can be connected with velocity disturbances generated by the main rotor vortex line moving relative to the tail rotor disk. In Fig. 15a,b are presented the changes of the in-plane and out-of-plane components of airflow of the tail rotor blade during passage the main rotor vortex line. the pass of vortex line in vicinity of the tail rotor in comparison with the side gusts created relatively smaller turn of fuselage (Fig. 16a,b), which are result of short period of time with strong influence of velocity induced by passing vortex line. The influence of velocity disturbances can be noticed at the time runs of the blade torsion deflection and angle of attack at tip of blade (Fig. 17a,b).

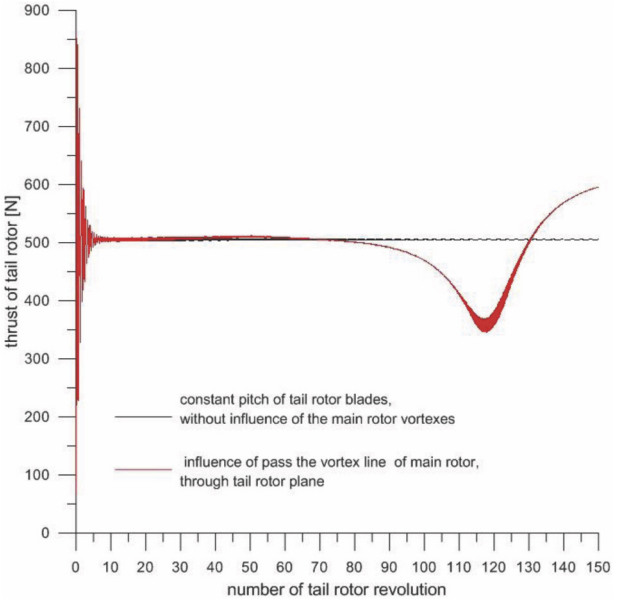

Fig. 13. Comparison of tail rotor thrust in conditions of flight at speed of $V = 10$ m/s with constant blade pitch without gusts of wind, for the case with no influence of the main rotor vortices and for the case of passing the main rotor vortex line through plane of tail rotor [Author, 2015]

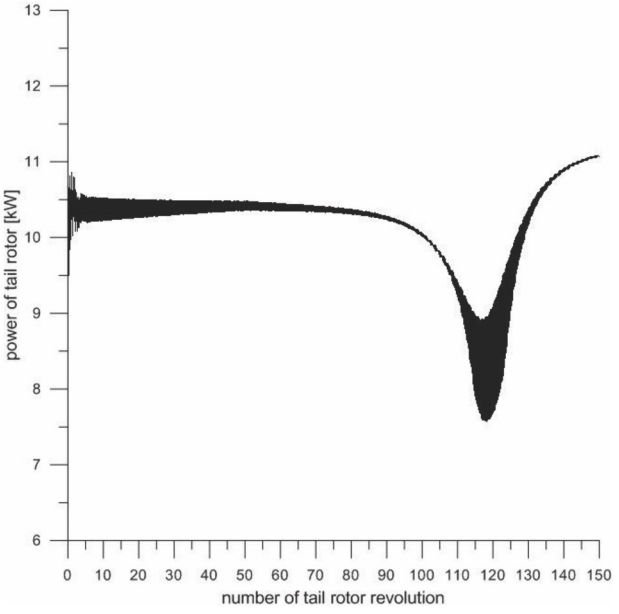

Fig. 14. Change of tail rotor power in flight at speed of $V = 10$ m/s with constant blade pitch, without gusts of wind for the case of passing the main rotor vortex line in vicinity of tail rotor disk [Author, 2015]

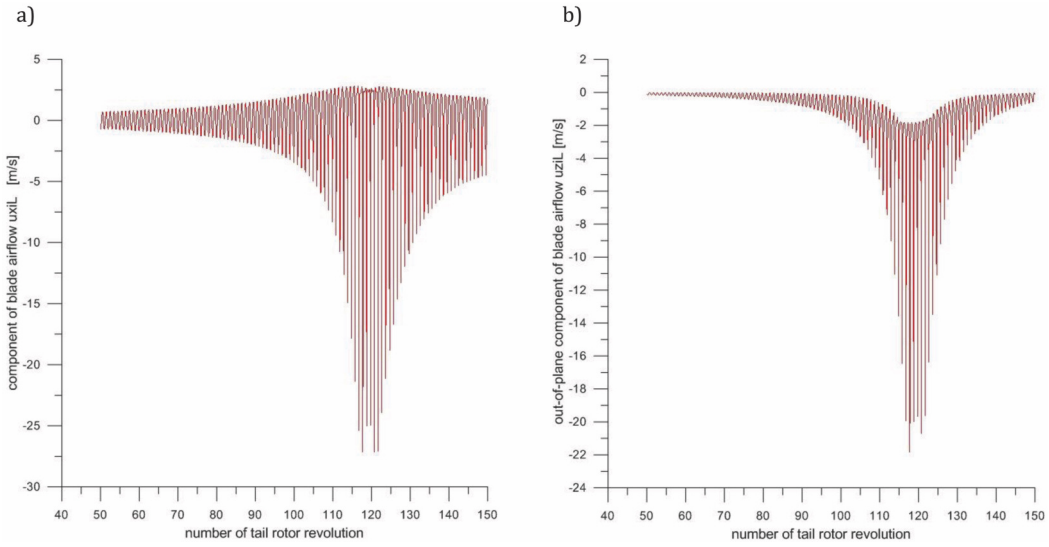

Fig. 15. Components of airflow at tip of tail rotor blade in flight at speed of $V = 10$ m/s during passing the main rotor vortex line in vicinity of tail rotor disk, constant pitch of tail rotor blades: a) component u_{xiL} in tail rotor plane, (-) direction coincident with rotation of blade causing reduction of its airflow speed; b) component u_{ziL} out of tail rotor plane, (-) direction coincident with induced velocity of tail rotor reducing attack angle of tail rotor cross-section [Author, 2015]

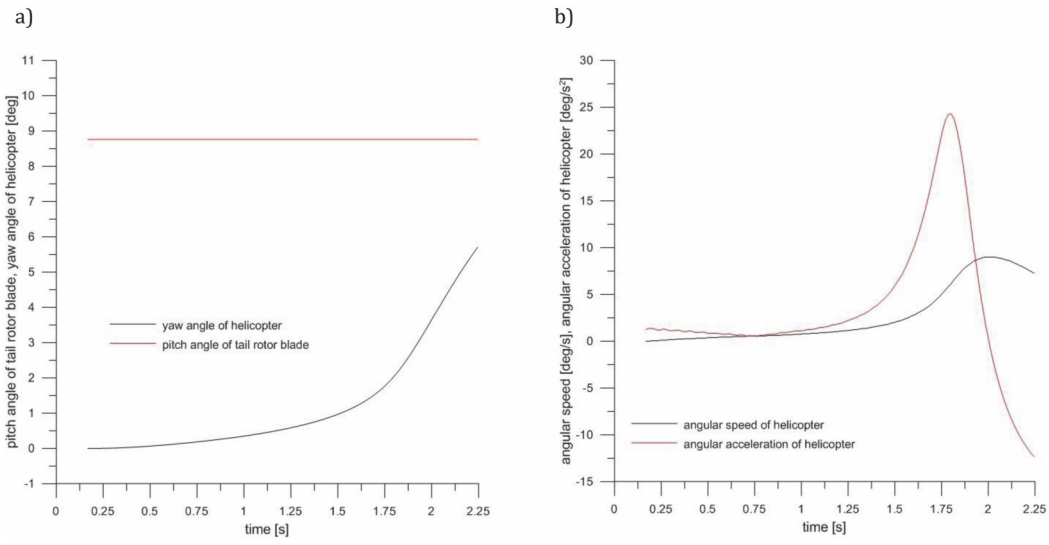

Fig. 16. Yaw angle (a), angular speed and acceleration of helicopter (b) in flight at speed of $V = 10$ m/s during passing the main rotor vortex line in vicinity of tail rotor disk. No action of pilot. Yaw angle (+) for fuselage nose turn to the right [Author, 2015]

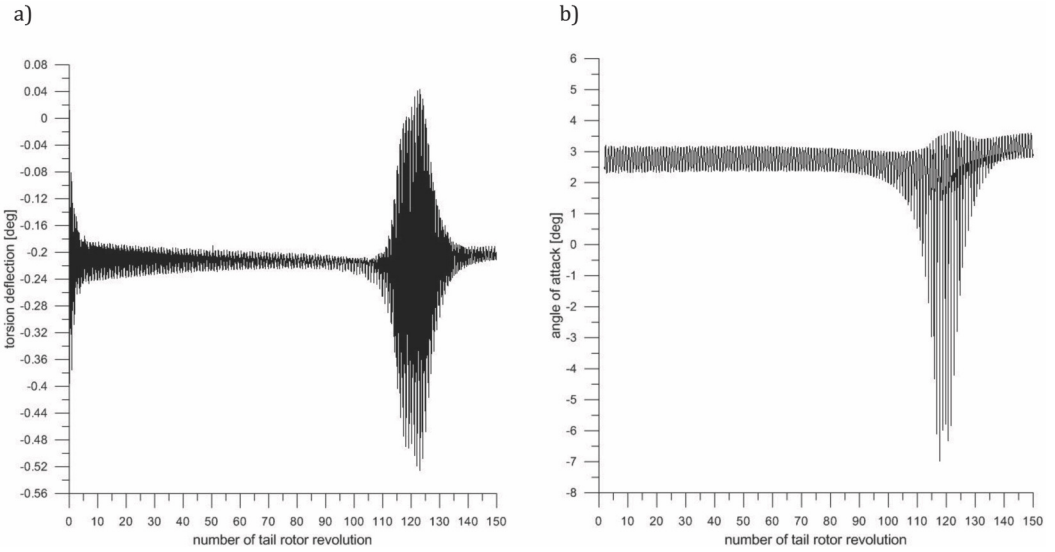

Fig. 17. Torsion deflection (a) and angle of attack (b) at tip of tail rotor blade for flight condition at speed of $V = 10$ m/s during passing the main rotor vortex line in vicinity of tail rotor disk. No action of pilot. Torsion deflection (-) for downward turn of nose of blade cross-section [Author, 2015]

The time runs of the tail rotor parameters in the directional maneuver in level flight at speed of $V = 10$ m/s with quick rate control of blade pitch are presented in Fig. 18÷20 for the case of initial decrease of pitch blade and in Fig. 21÷26 for the case with initial increase of the tail rotor blade pitch.

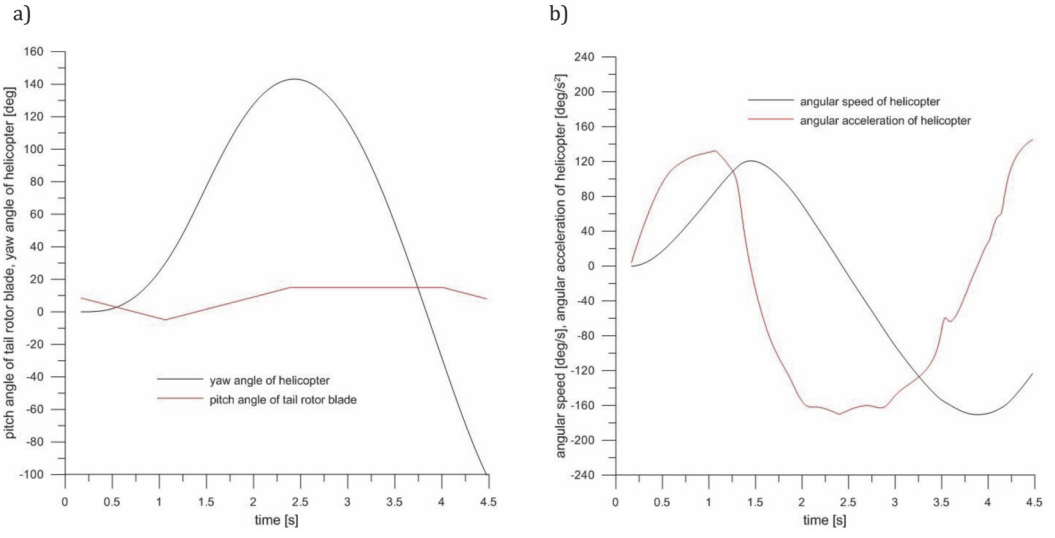

Fig. 18. Pitch control function of tail rotor blade and yaw angle of helicopter (a), angular speed and acceleration of helicopter (b) in directional maneuver in flight at speed of $V = 10$ m/s. Initially the blade pitch was decreased, when yaw of fuselage reached 30° the blade pitch was increased Yaw angle (+) for fuselage nose turn to the right. [Author, 2015]

The quick rate control of the blade pitch corresponds to the rapid move of pedals from balance position to limit and following return the pedals, when fuselage will reach the assumed yaw angle. The pedal movement in simulation program corresponds to the control function of the tail rotor blade pitch. It was assumed that full range of the pedal movement from the lower to the upper limit covers time of about two seconds, which corresponds the pitch rate of ~15°/s. The range of the tail rotor blade pitch covers from -8° to 15°.

In Fig. 18a is shown the control function of the blade pitch and time run of the fuselage yaw angle in the directional maneuver which cover 300 revolutions of tail rotor. Initially, in the simulation solution the blade pitch of the tail rotor was decreased, which caused reduction of the tail rotor thrust (Fig. 19a) and turn of helicopter to the right. The decrease of the blade pitch was continued till the assumed limit of the helicopter yaw $\beta_{f\_limit} = 30^{o}$ was reached. Then at the next time step the increase of the blade pitch started which was continued up to its maximum limit $\varphi_{tr} = 15^{o}$. The blade pitch of the tail rotor was kept at the maximum level till the helicopter reached the assumed limit of the yaw angle to the left $\beta_{f\_limit} = -30^{o}$. Applying the high rate of the tail rotor blade pitch causes the rapid change of the angular speed and acceleration of helicopter (Fig. 18b), thrust (Fig. 19a) and power of the tail rotor (Fig. 19b). During the directional maneuver the tail rotor disk passed through the zones of the large velocities generated by vortex lines of the main rotor. In the graphs of thrust and power of the tail rotor (Fig. 19a,b) can be noticed the changes due to the influence of vortex lines of the main rotor. The influence of the velocity disturbances generated by the main rotor vortex lines is also visible in the time runs of torsion deflection and angle of attack at the blade tip (Fig. 20a,b).

The parameters of the tail rotor in the directional maneuver for the reversed sequence of the control function of the blade pitch are shown in Fig. 21÷26. For the initial increase of the blade pitch to maximum level $\varphi_{tr} = 15^{o}$ the helicopter began the turn to the left. After reaching the assumed limit of the yaw angle $\beta_{f\_limit} = 30^{o}$ the blade pitch was decreased to minimum level $\varphi_{tr} = -8^{o}$ (Fig. 21a). For the decreased tail rotor thrust (Fig. 22a) the rotation of the helicopter to the left was continued with gradually lower-angular speed to the yaw angle of $\beta_{f} = -70^{o}$, next the helicopter started to yaw to the right. During the directional maneuver the influence of the velocity disturbances generated by the main rotor vortex lines is evident in time runs of thrust and power of the tail (Fig. 22a,b) and the time runs of the torsion deflection and attack angle at the blade tip (Fig. 23a,b). In Fig. 24 and 25 are shown fragments of the time run of torsion deflection at the blade tip for the range of the 68th÷78th tail rotor revolution (1.02÷1.17 second of simulation) at phase of maximum blade pitch kept before the main rotor vortex line approached the vicinity of the tail rotor area and at the 88th÷98th revolution the tail rotor (1.32÷1.47 second of simulation) in the phase of decreased the blade pitch during passage of the vortex line in the vicinity of the tail rotor. The vortex line of the main rotor in the close position to the tail rotor blade causes the growth of the blade torsion deflection and changes its distribution on the tail rotor disk. Initially similar to concentric circles shape of izolines in the map of the torsion blade deflections for the 68th tail rotor revolution (Fig. 24b) changes significantly at the 92nd revolution of the tail rotor (Fig. 25b) showing torsion oscillation of the blade. The time run and map of distribution of angle of attack for passage of the main rotor vortex line near the tail rotor (Fig. 26) show sharp change at the upper position of blade at azimuth 270° when the blade tip approaches the temporary location of the main rotor vortex line. Simulations of the directional maneuvers show that the large changes of thrust and power of the tail rotor due to the high rate of the blade pitch control shortens the time of passage of the vortex line in vicinity of the tail rotor which prevents its adverse influence. It must be noticed that even quick pass of tail rotor through the zone of velocity disturbances in a short time creates the large change of airflow conditions of the tail rotor blades and considerable growth of the tail rotor loads.

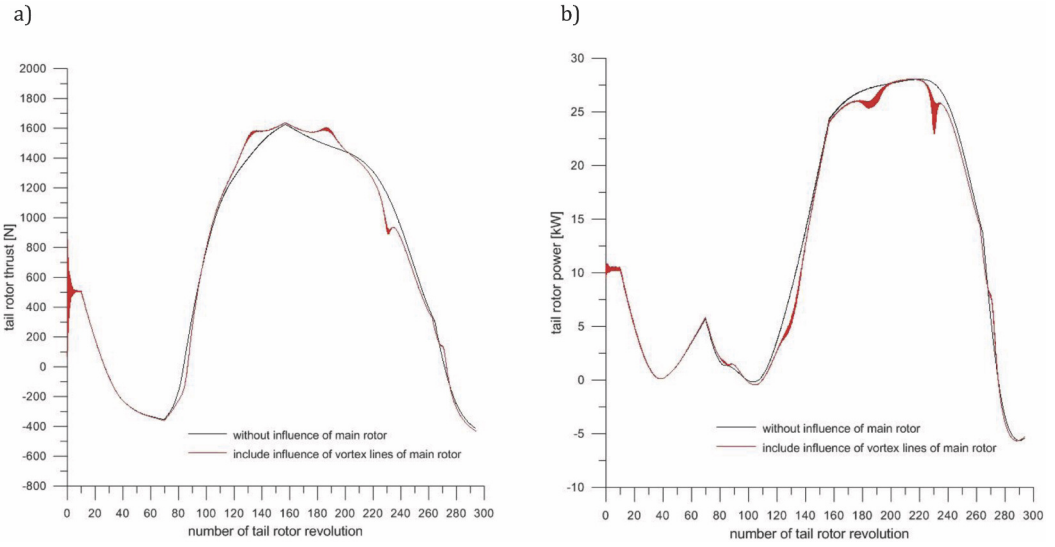

Fig. 19. Thrust (a) and power (b) of tail rotor in flight at speed of $V = 10$ m/s with quickly changed control function of blade pitch. Initially the blade pitch was decreased, when yaw of fuselage reached 30° the blade pitch was increased. Simulation without and including influence of main rotor vortex lines on induced airflow in area of tail rotor disk [Author, 2015]

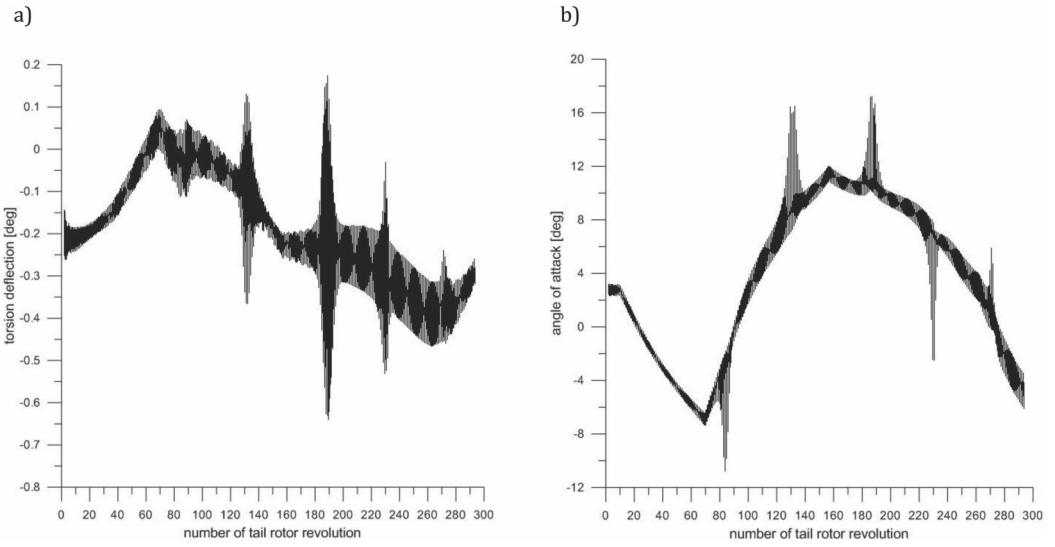

Fig. 20. Torsion deflection (a) and angle of attack (b) at tip of blade of tail rotor in helicopter directional maneuver in flight at speed of $V = 10$ m/s including influence of disturbances of airflow generated by the main rotor vortex lines during passage in vicinity of tail rotor disk. Initially the blade pitch was decreased, when yaw of fuselage reached 30° the blade pitch was increased [Author, 2015]

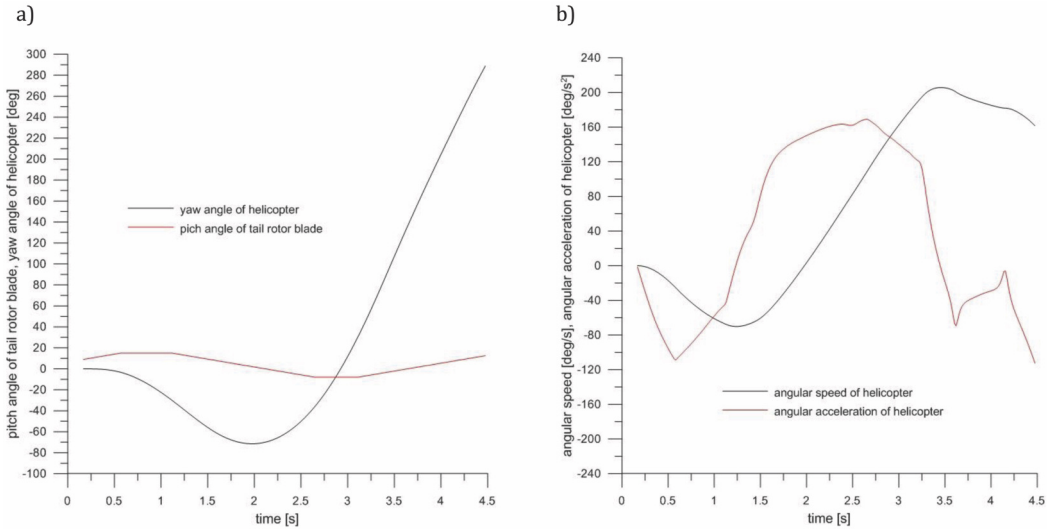

Fig. 21. Pitch control function of tail rotor blade and yaw angle of helicopter (a), angular speed and acceleration of helicopter (b) in directional maneuver in flight at speed of $V = 10$ m/s. Initially the blade pitch was increased, when yaw of helicopter in turn to the left reached 30° the tail rotor pitch was decreased Yaw angle (+) for fuselage nose turn to the right. [Author, 2015]

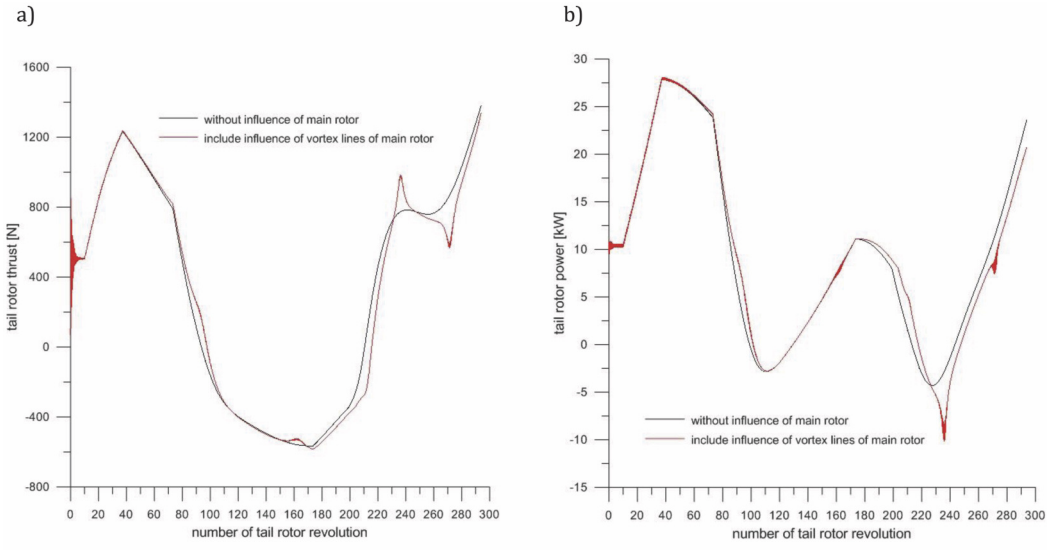

Fig. 22. Thrust (a) and power (b) of tail rotor in flight at speed of $V = 10$ m/s with quickly changed control function of blade pitch. Initially the blade pitch was increased, when yaw of fuselage reached 30° the blade pitch was decreased. Simulation for cases without and including influence of main rotor vortex lines on induced airflow in area of tail rotor disk. [Author, 2015]

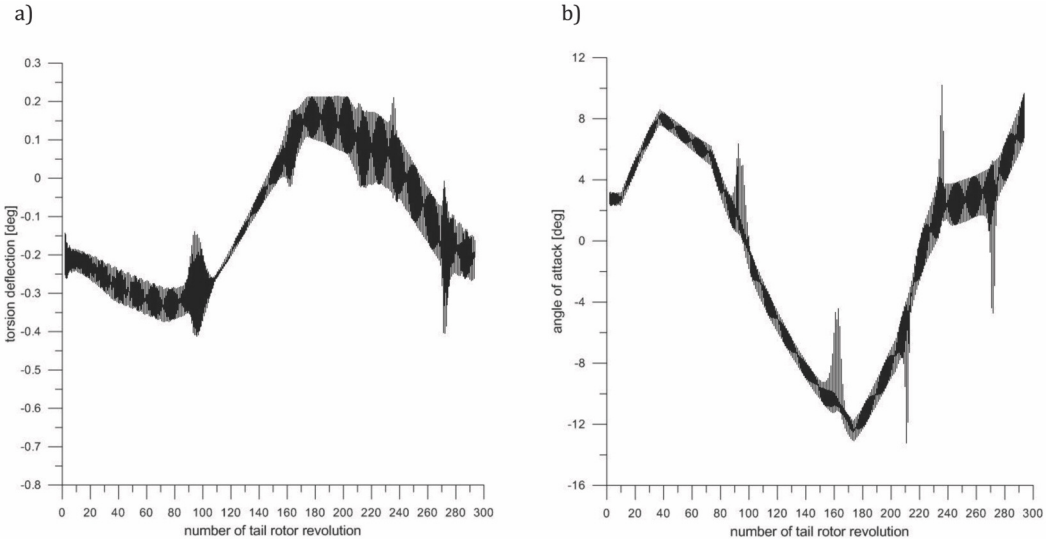

Fig. 23. Torsion deflection (a) and angle of attack (b) at tip of blade of tail rotor in helicopter directional maneuver in flight at speed of $V = 10$ m/s including influence of disturbances of airflow generated by the main rotor vortex lines during passage in vicinity of tail rotor disk. Initially the blade pitch was increased, when yaw of fuselage turning to the left reached 30° the blade pitch was decreased. [Author, 2015]

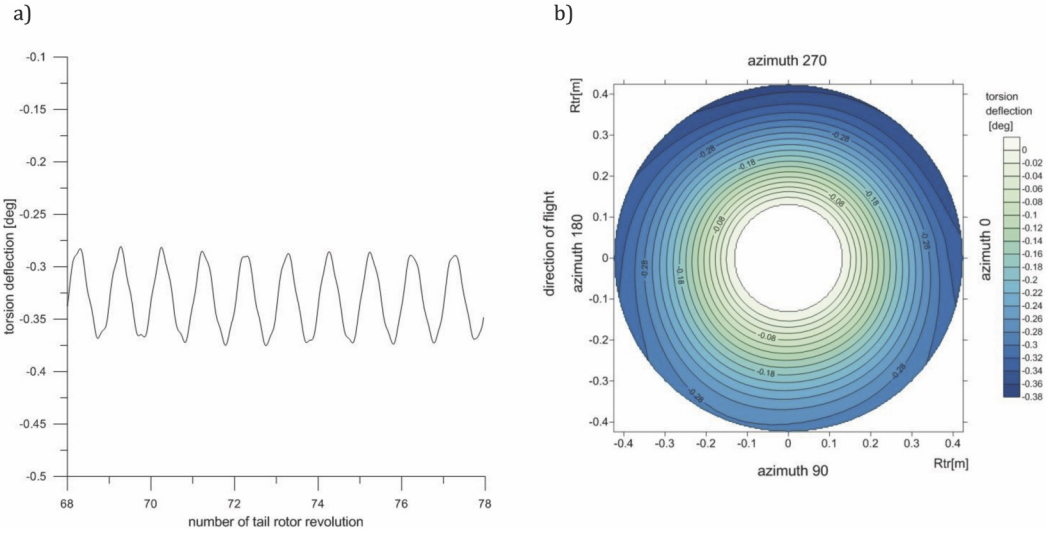

Fig. 24. Time run of torsion deflection (a) at tip of tail rotor blade, fragment of simulation for 68th-78th revolution of tail rotor in directional maneuver of helicopter in flight at speed of $V = 10$ m/s. Map of blade torsion deflection on tail rotor disk (b) for 68th revolution of tail rotor before passage of main rotor vortex line in vicinity of the tail rotor area. Initially the blade pitch was increased, when yaw of fuselage turning to the left reached 30° the blade pitch was decreased [Author, 2015]

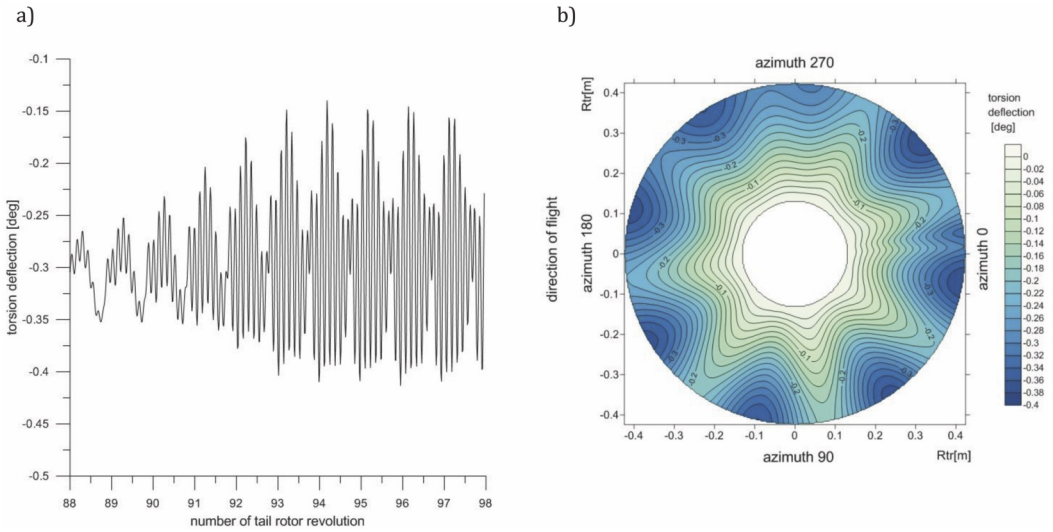

Fig. 25. Time run of torsion deflection (a) at tip of tail rotor blade, fragment of simulation for 88th-98th revolution of tail rotor in directional maneuver of helicopter in flight at speed of $V = 10$ m/s. Map of blade torsion deflection on tail rotor disk (b) for 92nd revolution of tail rotor at time of passage of main rotor vortex line near tail rotor area. Initially the blade pitch was increased, when yaw of fuselage turning to the left reached 30° the blade pitch was decreased [Author, 2015]

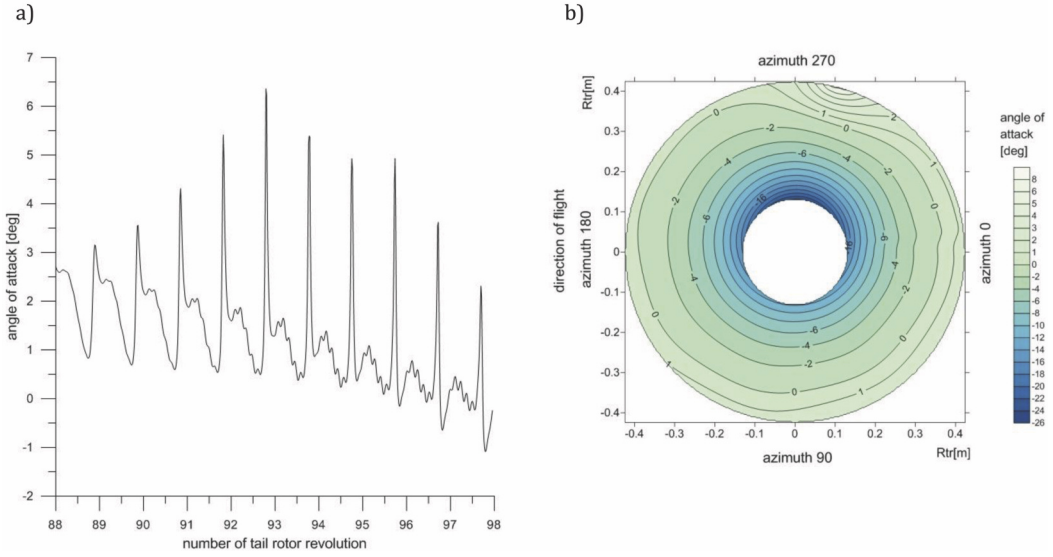

Fig. 26. Time run of attack angle (a) at tip of tail rotor blade, fragment of simulation for 88th-98th revolution of tail rotor in directional maneuver of helicopter in flight at speed of $V = 10$ m/s. Map of attack angle distribution on tail rotor disk (b) for 92nd revolution of tail rotor at time of passage of main rotor vortex line near tail rotor area. Initially the blade pitch was increased, when yaw of fuselage turning to the left reached 30° the blade pitch was decreased [Author, 2015]

4. CONCLUSIONS

The program code applying model of the elastic blade was prepared for the simulation investigation of the tail rotor behavior in directional maneuver of helicopter.

Program enables simulation of directional maneuver at given conditions of flight including effects of the side wind gusts, control of the tail rotor blade pitch and influence of airflow disturbances generated by vortex lines of the main rotor.

Simulations of the tail rotor work may aid to identify the circumstances of occurrence the phenomenon adverse affects the thrust and power of tail rotor.

The reduction of aerodynamic effectiveness of tail rotor in significant degree depends on period of time when the tail rotor blades remain in zone of strong disturbances of airflow.

For the considered cases of the helicopter directional maneuvers the results of calculations confirm possibility of loss of tail rotor effectiveness.

REFERENCES

[1] *Unanticipated Right Yaw in Helicopters*, 1995, Federal Aviation Administration, Advisory Circular, **90-95**.
[2] *Loss of Tail Rotor Effectiveness (LTE) on Unanticipated Yaw in Helicopters*, 2010, EASA Safety Information Bulletin, **2010-12R1**.
[3] *Safety Considerations, Training Leaflet HE1*, 2010, EASA European Helicopter Safety Team (EHEST).
[4] *Rotorcraft Flying Handbook*, 2000, Federal Aviation Administration, FAA-H-8083-21, Chap. 11.
[5] *Requirements and Guidance Material for Operators*, 2011, UK CAA-CAP 7892011, Miscellaneous Provisions Affecting Helicopter Operation, Chap. 21.
[6] Learmont, D., 2004, "Sting in the Tail," Flight International, pp. 40-41.
[7] *Loss of Tail-rotor Effectiveness Cited in Bell 206B Accident During Videotaping Flight*, 2005, Helicopter Safety – Flight Safety Foundation, **31**(1).
[8] Brown, W., 2004, "Basics and Professionalism," Heliprops – Helicopter Professional Pilot Safety Program, **16**(3).
[9] *Helicopter loss of Tail Rotor Effectiveness*, 2011, U.S. Forest Service Interagency Aviation Safety Alert, **11-03**.
[10] Cuzieux, F., Basset, P., and Desopper, A., 2012, "Modeling of Loss of Tail Rotor Effectiveness Conducting to Unanticipated Yaw," *28th International Congress of the Aeronautical Sciences ICAS 2012*, Brisbane, Australia.

SYMULACYJNE BADANIE ZMNIEJSZENIA AERODYNAMICZNEJ EFEKTYWNOŚCI ŚMIGŁA OGONOWEGO ŚMIGŁOWCA

Streszczenie

Przedstawiono wyniki obliczeń symulacyjnych dotyczących pracy śmigła ogonowego w manewrze kierunkowym śmigłowca z uwzględnieniem zmiennych warunków opływu łopat śmigła. W modelu obliczeniowym uwzględniono ruch obrotowy sztywnego kadłuba oraz parametry pracy odkształcalnych łopat śmigła ogonowego traktowanych jako osie sprężyste z przypisanym rozkładem mas skupionych. Równania ruchu łopat rozwiązywano metodą Runge-Kutta z uwzględnieniem giętnych i skrętnych postaci własnych łopat. Wykonane obliczenia wskazują na możliwość wystąpienia znacznych zmian ciągu rozwijanego przez śmigło ogonowe w szczególnych przypadkach realizacji manewru kierunkowego przy podmuchach bocznych lub przy oddziaływaniu zaburzeń opływu pochodzących od wirnika nośnego.
Słowa kluczowe: śmigłowiec, śmigło ogonowe, efektywność aerodynamiczna.